Geochemical Perspectives Letters

Tungsten isotopes in Baffin Island lavas: Evidence of Iceland plume evolution

J. Kaare-Rasmussen, D. Peters, H. Rizo, R.W. Carlson, S.G. Nielsen, F. Horton

Supplementary Information

The Supplementary Information includes:

1. Analytical Methods

Glassy pillow rinds were cut from samples using a diamond-bit rock saw. Sawn surfaces were sanded away using silica-carbide-grit paper to remove any metal contamination from the saw. Samples were then crushed using metal-free tools (rubber mallets, ceramic mortar and pestle) to avoid metal contamination. Under a binocular microscope, 11.54–12.36 g of clean glass chips were picked by hand to avoid palagonite. Samples were then dissolved in new, clean, Savillex Teflon beakers using a mixture of ultrapure (pg g^{-1}-level) concentrated HF-HNO_3 reagents, followed by repeated dry downs and redissolutions in concentrated HNO_3. Finally, samples were dried down and dissolved in 6 M HCl.

A ~5 % mass aliquot was separated from the samples in 6 M HCl solution to analyse W concentrations *via* isotope dilution. Sample aliquots (~0.5 g total) were spiked with a ^{186}W tracer, dried down, and re-

dissolved to achieve sample-spike equilibrium. Tungsten was isolated using ion chromatography as described in Nagai and Yokoyama (2014). Tungsten concentration measurements were performed using the ThermoFisher Neptune multicollector ICP-MS at the Department of Earth Sciences of Carleton University (Ottawa, Canada).

For high-precision isotope ratio analyses, W was separated from the remaining non-spiked 95 % aliquots using three column steps. The first column, filled with 20 mL of AG50W-X8 (200–400 mesh) resin, separated W and other high field strength elements (HFSE) from the rock matrix in a procedure similar to that described in Touboul and Walker (2012). The second column, filled with 10 mL of AG1-X8 (200–400 mesh) resin, separated W from other HFSEs, as well as any remaining Ti and Al, as described in Breton and Quitté (2014). Finally, the samples passed through a third clean-up column with 0.3 mL AG1-X8 (200–400 mesh) to remove any remaining Ti, which can hinder W ionisation efficiency (Touboul and Walker, 2012). Purified W solutions were redissolved with a drop of concentrated HNO_3-HCl-H_2O_2 several times in open Savillex beakers at 150 °C before being redissolved in 0.5 N HCl – 0.5 N HF and loaded onto single degassed zone-refined rhenium filaments. Tungsten blanks were <4 ng and yields were greater than ~50 %.

Tungsten isotopes were measured as WO_3^- anions on the ThermoFisher Triton thermal ionisation mass spectrometer (TIMS) at the Department of Earth Sciences of Carleton University (Ottawa, Canada). Loaded W amounts were 346–1323 ng for the unknowns. Tungsten oxides were produced and ionised using a La-Gd activator solution and O_2 bled into the TIMS source at a source pressure of approximately 1.15×10^{-7} mbar. Tungsten isotopes were measured using a protocol similar to the one described in Archer *et al.* (2017), in which dominant oxides (*e.g.*, $W^{16}O_3^-$) were measured on Faraday cups connected to 10^{11} Ω amplifiers. Trace oxides, such as $^{186}W^{16}O_2{}^{18}O^-$, were measured with Faraday cups coupled to 10^{12} Ω amplifiers. Measurements were performed using a multistatic method with three steps, during which $^{184}WO_3$, $^{185}ReO_3$ and $^{186}WO_3$ were sequentially measured with the axial detector. Step 1 had an integration time of 33 s and an idle time of 12 s to allow for low-noise measurements of $^{186}W^{16}O_2{}^{18}O^-$ and $^{187}Re^{16}O_2{}^{18}O^-$ using a 10^{12} Ω amplifier. Acquisition

cycles 2 and 3 did not measure the trace oxides and therefore had a collection time of 8 s and an idle time of 4 s. Individual W isotope analyses contain 173–640 cycles (averaging 400 cycles per analysis), divided into 20-cycle blocks. Throughout the analytical session, 1200 s baselines were obtained every 7 blocks. Peak centring and lens focusing were repeated every 3 blocks to minimise drift. Steps 1 and 2 were averaged to calculate mean $^{182}W/^{184}W$ and $^{183}W/^{184}W$ ratios. All W isotopic ratios have been corrected for instrumental fractionation using the $^{186}W/^{184}W$ ratio of 0.92767 (Völkening *et al.*, 1991) and O isotopic compositional relations from Archer *et al.* (2017). Results are reported in μ-notation relative to the Alfa Aesar W reference material. The weighted mean isotopic composition of 500 ng and 1000 ng aliquots the Alfa Aesar reference material was $^{182}W/^{184}W = 0.864888 \pm 0.000006$ (2 s.e., $n = 8$) and $^{183}W/^{184}W = 0.467151 \pm 0.000004$ (2 s.e., $n = 8$).

To assess measurement accuracy and repeatability, 500 ng aliquots of the National Institute of Standards and Technology (NIST) W isotope standard solution 3163 was repeatedly measured throughout the analytical session. Normalised to the Alfa Aesar reference material, NIST 3163 yielded $\mu^{182}W = +2.0 \pm 5.8$ (2 s.d., $n = 4$) and $\mu^{183}W = -0.6 \pm 7.7$ (2 s.d., $n = 4$), which agree with literature values (Kruijer *et al.*, 2012).

2. Methodology Developments

Rizo *et al.* (2016) reported $\mu^{182}W$ excesses ranging from +10 to +48 in Baffin Island lavas. This section discusses the acquisition methodology of Touboul and Walker (2012) and speculates about causes for the discrepancy between the results of Rizo *et al.* (2016) and this study.

Rizo *et al.* (2016) utilised the W isotope measurement techniques outlined in Touboul and Walker (2012), which involve N-TIMS analyses of WO_3^- species using Faraday collectors equipped with 10^{11} Ω amplifiers. The measured W isotopic ratios were corrected for instrumental mass fractionation using the $^{186}W/^{184}W$ ratio. The fractionation-corrected $^{182}W/^{184}W$ and $^{183}W/^{184}W$ exhibit residual positive correlations that were attributed to mass-dependent fractionation of oxygen isotopes (Touboul and Walker, 2012). To

determine the $^{182}W/^{184}W$ ratio, a second-order correction was necessary using an assumed natural $^{183}W/^{184}W$ ratio of 0.467151 (Fig. S-1).

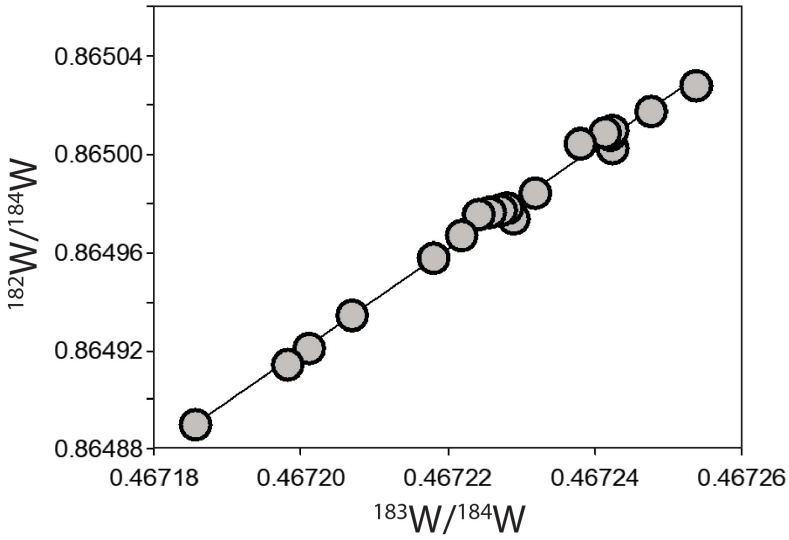

Figure S-1 Explanatory diagram of $^{182}W/^{184}W$ and $^{183}W/^{184}W$ illustrating how $^{182}W/^{184}W$ ratios were determined in Rizo *et al.* (2016). Correlated $^{182}W/^{184}W$ and $^{183}W/^{184}W$ ratios of W standards were obtained after instrumental mass fractionation using the $^{186}W/^{184}W$ ratio. The final $^{182}W/^{184}W$ was obtained by assuming a natural $^{183}W/^{184}W$ ratio of 0.467151.

N-TIMS methodology for W isotope ratio determinations improved when Archer *et al.* (2017) developed a procedure for measuring the oxygen isotopic composition of WO_3^- molecules. This involved equipping two Faraday detectors with 10^{12} Ω amplifiers, which enabled measurements of low abundance W oxides (*e.g.*, $^{186}W^{16}O_2{}^{18}O$ ion beams are typically ~5 mV). By measuring, for example, $^{186}W^{16}O_3$ and $^{186}W^{16}O_2{}^{18}O$ molecules, precise measurements of oxygen isotopic compositions can be obtained (Fig. S-2). This permits a correction for oxygen isotopic fractionation during the analysis and thereby eliminates the need

for a second-order W isotopic correction. As a result, direct measurement of $^{183}W/^{184}W$ became possible with a similar level of precision as $^{182}W/^{184}W$.

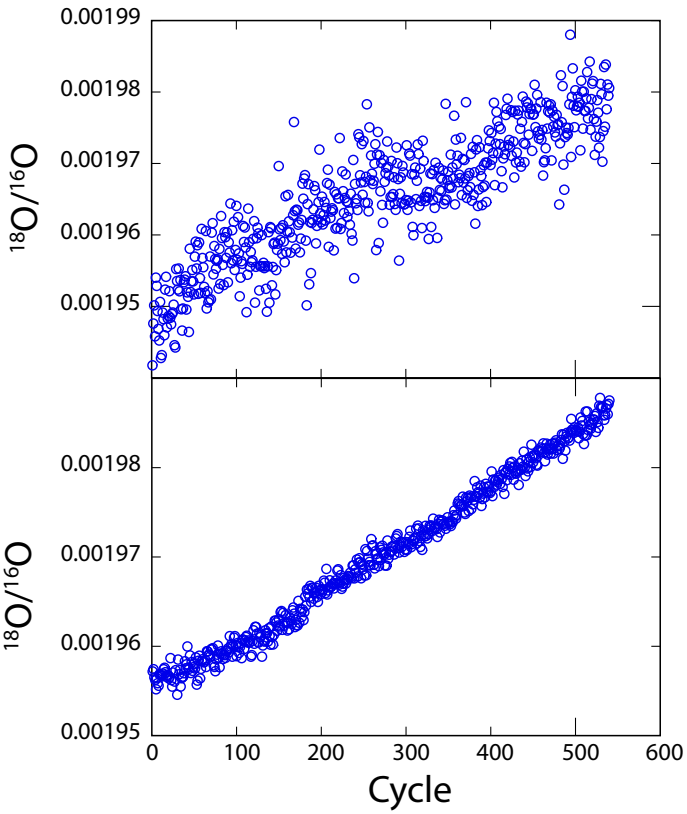

Figure S-2 Oxygen isotopic compositions change during individual analyses. (Top) The oxygen isotopic evolution during measurements of a standard using standard 10^{11} Ω amplifiers. (Bottom) The same as above but with 10^{12} Ω amplifiers, which amplify the signal/noise ratio by a factor of 3.

The ^{182}W excesses reported by Rizo *et al.* (2016) have been attributed to nuclear field shift effects (*e.g.*, Kruijer and Kleine, 2018). However, analysis of Baffin Island lavas with improved N-TIMS methods indicates that these rocks lack $^{183}W/^{184}W$ anomalies, which is inconsistent with nuclear field shifts. Evidence of nuclear

field shifts has not emerged from the growing dataset produced using the same N-TIMS methodology (Archer *et al.*, 2017; Mundl *et al.*, 2017; Rizo *et al.*, 2019; Mundl-Petermeier *et al.*, 2020; Nakanishi *et al.*, 2023).

The source of ^{182}W excesses reported by Rizo *et al.* (2016) remains uncertain. Contamination from a ^{186}W spike may have produced high $^{182}W/^{184}W$ ratios. Reducing Rizo *et al.* (2016) data for sample Pd-2 using $^{183}W/^{184}W$ for fractionation correction instead of $^{186}W/^{184}W$ yields a $\mu^{182}W$ of −14 and a $\mu^{186}W$ of +146, which may be consistent with spike contamination. Mixing as little as 7 pg of W from the ^{186}W spike into that sample could have produced the high $\mu^{186}W$ value. Alternatively, an atypical oxygen isotopic composition during the analysis may have caused artificially high $^{182}W/^{184}W$ measurements. Assuming sample Pd-2 had $\mu^{182}W \approx 0$, the $\delta^{18}O$ of the sample would have been 20–27 ‰ lighter than the Nier values of the standards. If so, inaccurate oxygen isotopic corrections can explain the $\mu^{182}W$ excesses. In any case, the improved N-TIMS methodology employed in this study overcomes previous limitations and more accurately constrains Baffin Island lava $\mu^{182}W$.

3. Crustal Contamination

Continental crust assimilation may affect the $\mu^{182}W$ compositions of lavas. Tungsten is incompatible during mantle melting and is therefore enriched in continental crust relative to the mantle. Thus, assimilated continental crust could dominate the W budget of a mafic magma and overprint intrinsic $\mu^{182}W$ anomalies. This is especially true for Archean crust with positive $\mu^{182}W$ anomalies that might mask any core-derived $\mu^{182}W$ signature (Reimink *et al.*, 2020, and references therein). In this case, the observation of negative $\mu^{182}W$ in Iceland but not Baffin Island lavas might reflect the masking of a negative $\mu^{182}W$ plume component by assimilated crust in the Baffin Island only.

The Baffin Island lavas erupted through the southeastern margin of the Rae Craton (St-Onge *et al.*, 2009, 2020). Variability in radiogenic isotopes (Sr, Nd and Pb) and trace element ratios (Nb/Th, Ce/Pb) implies the Baffin Island lavas and conjugate western Greenland lavas assimilated variable amounts of

continental crust (Larsen and Pedersen, 2009; Willhite *et al.*, 2019). Willhite *et al.* (2019) showed that the Baffin Island lavas with the most radiogenic $^{143}Nd/^{144}Nd$ and least radiogenic $^{87}Sr/^{86}Sr$ ratios in the Baffin Island lava suite did not experience significant assimilation of crustal material. Using a range of crustal compositions, they were unable to simultaneously replicate the whole rock radiogenic isotope compositions and trace element ratios in two component mixing between crustal compositions and the primitive magmas erupting in the modern Iceland plume. Their work provides useful geochemical context for placing bounds on the extent of crustal contamination in the Baffin Island lavas analysed for W isotopes.

Whereas most radiogenic $^{143}Nd/^{144}Nd$ and least radiogenic $^{87}Sr/^{86}Sr$ ratios measured in the Baffin Island lavas may approximate the composition of the primary magmas ($^{87}Sr/^{86}Sr$ = 0.702995 and $^{143}Nd/^{144}Nd$ = 0.513174: Willhite *et al.*, 2019), their Nd and Sr concentrations—dependent on the extent of melting and fractional crystallisation—are uncertain. We assume a lower limit ([Sr] = 7.664 μg g^{-1} and [Nd] = 0.581 μg g^{-1}; Workman and Hart, 2005) equal to depleted MORB mantle (DMM) and an upper limit equal to the least-contaminated Baffin Island lavas ([Sr] = 48.9 μg g^{-1} and [Nd] = 2.42 μg g^{-1}; Willhite *et al.*, 2019). We further assume that the assimilated crust had a composition similar to Precambrian shales in western Greenland (sample 113450, [Sr] = 192.81 μg g^{-1}, [Nd] = 47.931 μg g^{-1}, $^{87}Sr/^{86}Sr$ = 0.721081, and $^{143}Nd/^{144}Nd$ = 0.5111164; Larsen and Pedersen, 2009). Based on our lower and upper limits for primary magma [Nd] and [Sr], $^{143}Nd/^{144}Nd$ and $^{87}Sr/^{86}Sr$ variability in our dataset can be explained by ≤0.2 % or ≤1 % crustal assimilation, respectively.

The sensitivity of magmas to $\mu^{182}W$ overprinting depends on the composition of the primary magmas, as well as the crust. A $\mu^{182}W$ anomaly of the same magnitude as those measured in Iceland (−12.6; Mundl-Petermeier *et al.*, 2019) can be fully overprinted by the assimilation of 6 % crust with $\mu^{182}W$ = 0 or 0.65 % Archean crust with $\mu^{182}W$ = +20, assuming that the assimilated crust has W concentrations equal to average upper continental crust (1.9 μg g^{-1}; Rudnick and Gao, 2003). If the Sr and Nd isotope systematics only allow for at most 0.2 % crustal assimilation, then even Archean crust cannot overprint a $\mu^{182}W$ anomaly of −12.6.

However, 1 % Archean crust assimilation could entirely mask this $\mu^{182}W$ composition. Better constraints for Baffin Island basement are necessary to further constrain the potential overprinting effects. Therefore, we cannot rule out the possibility that the Baffin Island mantle source contains negative $\mu^{182}W$ anomalies that were overprinted during crustal assimilation.

Nonetheless, the lack of correlation among elemental and isotopic ratios in Baffin Island lavas implies that W isotopic overprinting in our samples is unlikely. Willhite *et al.* (2019) proposed a series of filters for crustal assimilation in Baffin Island lavas. They propose that samples with >10 wt.% MgO, Nb/Th > 13 and Ce/Pb > 20 have minimal crustal contamination. Only one of our samples fit into the least-contaminated sample set, based on these criteria (RB18-H3); the rest pass at least one of the three filters. If $\mu^{182}W$ is a function of crustal assimilation, we would expect to see correlation between $\mu^{182}W$ and other assimilation tracers (*e.g.*, MgO, Ce/Pb, Nb/Th, or $^{87}Sr/^{86}Sr$ and $^{143}Nd/^{144}Nd$ ratios) because our samples contain evidence for variable degrees of crustal assimilation. Importantly, within our sample set there is no correlation between $\mu^{182}W$ and crustal assimilation tracers such as MgO, Ce/Pb, Nb/Th, or $^{87}Sr/^{86}Sr$ and $^{143}Nd/^{144}Nd$ ratios. Thus, although it is possible the $\mu^{182}W$ we report for Baffin Island lavas is the result of crustal assimilation, it would require the basement rocks to have a positive $\mu^{182}W$ anomaly or much more crustal assimilation (~6 %) than the radiogenic isotopes and trace element ratios permit. More likely, the $\mu^{182}W$ reported here is representative of the mantle plume.

4. Calculating Diffusion in the Long-term Stable Mantle Plume Source

Isotopic diffusion across the CMB is a function of the isotopic compositions of the core (c_c) and mantle (c_m), time (t), and diffusivity (D). Isotopic diffusion can be approximated using Fick's second law as $\frac{\partial c}{\partial t} = D\frac{\partial^2 c}{\partial x^2}$, where x is the distance from the core. Under the assumption that the core and mantle are infinite isotopic reservoirs, a one-dimensional concentration gradient across the core-mantle boundary can be calculated from

the general solution of Fick's second law as $c(x,t) = c_c - (c_c - c_m)\mathrm{erf}\left(\frac{x}{2\sqrt{Dt}}\right)$. The error function (erf[z]) is calculated by $\mathrm{erf}(z) = \frac{2}{\sqrt{\pi}}\int_0^z e^{-t^2}dt$. Fick's second law predicts the diffusion gradient changes with time. Therefore, we use a constant time (1 Gyr) to calculate $c(x, 1\ \mathrm{Gyr})$ for x along the length of stable structures at the CMB, where $c_{(c,\,W)} = -200$ (*e.g.*, Rizo *et al.*, 2019), $c_{(m,\,W)} = 0$, $c_{(c,\,He)} = 120$ Ra (*e.g.*, Atreya *et al.*, 2003), $c_{(m,\,He)} = 8$ Ra (*e.g.*, Moreira and Kurz, 2013). The diffusivities of W and He are poorly constrained. Under the assumption that diffusivities are not pressure dependent, D_W and D_{He} were extrapolated from experimentally determined diffusivities at standard temperature and pressure ($D_W = 4.62 \times 10^{-10}$ m^2 s^{-1} and $D_{He} = 10^{-10}$ m^2 s^{-1}; Hart *et al.*, 2008; Yoshino *et al.*, 2020; Ferrick and Korenaga, 2023) using the Arrhenius equation $D = D_0 e^{-E_A/RT}$, where D_0 is the diffusivity, E_A is the activation energy, T is the temperature at the core-mantle boundary (4000 K), and R is the gas constant. Tungsten volume diffusion is expected to negligible (*e.g.*, Yoshino *et al.*, 2020), so we consider $D_{W,0}$ as solely grain boundary diffusion calculated using the assumptions in Ferrick and Korenaga (2023). Helium volume diffusion in olivine is relatively slow and offers a good lower bound for the diffusivity of He, which we use for $D_{He,0}$ after Hart *et al.* (2008). Nevertheless, this exercise demonstrates that He and W might be mobile over large enough regions in the lowermost mantle to influence plumes that originate near the CMB, and that He and W might be kinetically fractionated. This model suggests that core-like ^{3}He/^{4}He can be transported farther from the CMB than negative μ^{182}W anomalies, but the diffusion limits for He and W are so uncertain that we plot distance from the CMB as unitless in Figure 2.

5. Diffusion Calculations in the Convecting Mantle

The diffusion of W from the core into the mantle might explain the inferred μ^{182}W decline of ~27 in the convecting mantle. Mantle μ^{182}W evolution is dependent on the timescales of convecting mantle residence on the CMB (residence time, τ) and the percentage of the CMB that is insulated by long-term stable structures (ξ). We envisage a scenario in which conveyor belts of convecting mantle are in contact with the core, except

where stable structures exist, and that the isotopic anomalies acquired *via* diffusion from the core are efficiently mixed into the rest of the convecting mantle (*i.e.,* the entire mantle minus the long-term structures at the CMB). We first calculate how many unique parcels of convecting mantle were exposed to the core by dividing the duration of mantle convection (assumed to be 4.5 Gyr) by τ. For example, if τ = 100, there have been 45 unique parcels of mantle on the CMB. Next, we calculate the volume of the convecting mantle into which core-like $\mu^{182}W$ diffused. To do this, we multiply the CMB area exposed to the convecting mantle (the surface area of the core × ξ) by the characteristic diffusion length scale ($\sqrt{D\tau}$ where D is diffusivity). We assume that (a) this volume acquired core-like $\mu^{182}W$ during its residence at the CMB (*e.g.*, Ferrick and Korenaga, 2023) and (b) it mixes efficiently into the convecting mantle. After each unique parcel cycle, we calculate the average convecting mantle $\mu^{182}W$.

Convection rates in the ancient mantle are a major source of uncertainty for this model. Giant impacts, the rise of modern plate tectonics, and secular cooling of the mantle likely influenced convection rates. Therefore, we calculated different paths through mantle $\mu^{182}W$-time space with varying mantle convection rates. A first-order question is what τ can fully explain the ~27 decrease in average mantle $\mu^{182}W$. We modelled a constant decrease in average mantle $\mu^{182}W$ using τ = 35 Myr in the dashed line (Fig. 3b). Such a quick refresh rate can explain the mantle decrease through time; however, this does not fit the published Archean data well. Ferrick and Korenaga (2023) assumed that τ ≈ 100 Myr in the modern Earth, but poor constraints exist for this value. We also modelled two other end-member cases, one where there is a steep decrease in a rapidly convecting mantle early in Earth history (τ = 0.1 Myr) in a whole mantle magma ocean scenario. Then a constant τ = 200 Myr. τ is expected to increase as the mantle cools. Gradual cooling might lead to a gradual increase in τ, which fits the lower bound of published Archean data well. Finally, there is evidence for a sharp change in $\mu^{182}W$ near the end of the Archean (*e.g.*, Nakanishi *et al.*, 2023). This may be emblematic of the initiation of modern plate tectonics, which we model with a sharp decrease in $\mu^{182}W$ around 3 Ga (τ = 0.4 Myr). This path (dotted line in Fig. 3b) fits the upper end of published Archean $\mu^{182}W$ data.

Supplementary Tables

Table S-1 Isotopic compositions of the standards. Both $\mu^{182}W$ and $\mu^{183}W$ are reported as μg g^{-1} deviations from the average Alfa Aesar standard ($^{182}W/^{184}W$ = 0.864888 ± 0.000006 and $^{183}W/^{184}W$ = 0.467151 ± 0.000004, 2 s.e., n = 8), respectively. Both $\mu^{182}W$ and $\mu^{183}W$ are normalised to $^{186}W/^{184}W$, denoted by subscript 6/4. The internal run precision of each individual analyses is reported as 2 s.e.

Sample	$\mu^{182}W_{6/4}$	2 s.e.	$\mu^{183}W_{6/4}$	2 s.e.
Alfa Aesar 1-4	−2.0	5.6	−4.8	4.5
Alfa Aesar 1-5	0.5	5.3	2.9	4.4
Alfa Aesar 1-6	−4.7	7.1	−5.5	6.3
Alfa Aesar 2-2	0.3	7.8	0.5	6.1
Alfa Aesar 2-3	0.2	9.0	-3.7	8.1
Alfa Aesar 2-5	−4.6	6.5	−1.3	5.9
Alfa Aesar 3-4	3.7	4.8	4.0	4.2
Alfa Aesar 3-5	3.7	4.8	3.7	4.1
NIST 3163-1	5.1	7.0	4.7	6.4
NIST 3163-2	−0.2	5.7	−2.3	5.1
NIST 3163-3	3.0	5.2	−3.6	4.7
NIST 3163-4	−1.2	5.6	−3.3	4.7

Table S-2 Elemental concentration from the Baffin Island lavas. Starred samples produced usable $\mu^{182}W$ data. Helium isotopic compositions are the highest reproducible ratios from Horton *et al.* (2023), normalised to the atmospheric ratio of 1.384×10^{-6} (Ra).

Sample	[W] (ng g^{-1})	[Th] (ng g^{-1})	[U] (ng g^{-1})	$^3He/^4He$ (Ra)	2 s.e.
DURB18-H4	21.8	93.4	23.3	-	-
DURB18-H11*	20.9	91.3	24.2	39.0	3.5
PING18-H2*	107.0	443.0	102.3	65.9	3.4
PING18-H3	30.9	118.3	31.9	43.9	1.4
PING18-H16*	90.6	105.0	71.4	-	-
PING18-H19	78.6	325.9	58.7	-	-
PING18-H20*	85.3	302.2	70.0	-	-
RB18-H3*	26.2	292.8	34.1	36.3	8.9

Supplementary Figures

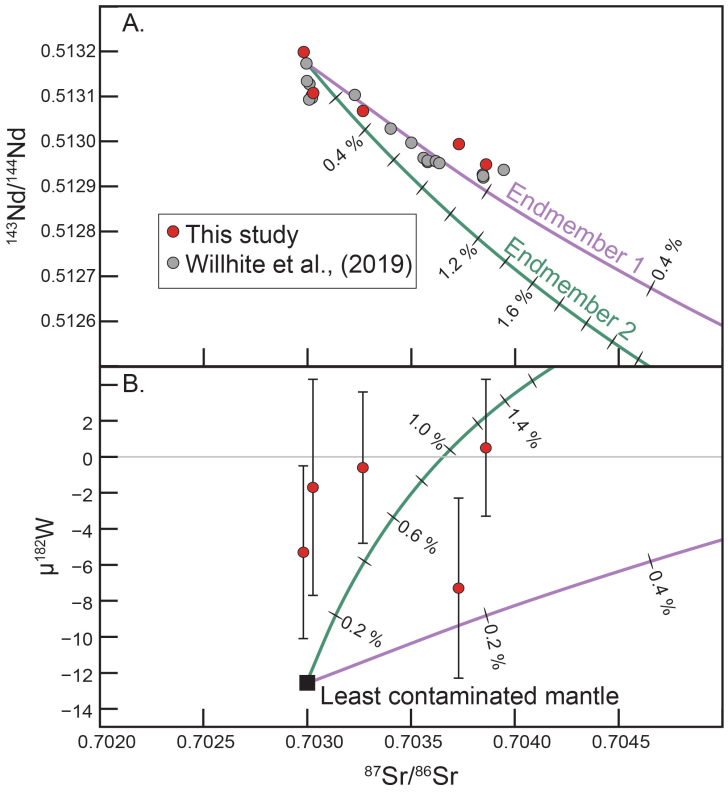

Figure S-3 Mixing models between uncontaminated mantle and the assumed Precambrian basement of Baffin Island ($\mu^{182}W = +20$, [W] = 1.9 μg g^{-1}, [Sr] = 192.81 μg g^{-1}, [Nd] = 47.93 μg g^{-1}, $^{87}Sr/^{86}Sr = 0.721081$, $^{143}Nd/^{144}Nd = 0.5111164$; based on sampled 113450 from Rudnick and Gao, 2003; Larsen and Pedersen, 2009; Willhite *et al.*, 2019). Mixing is strongly dependent on Sr and Nd concentrations in the mantle. Endmember 1 (purple) assumes mantle concentrations ([Sr] = 7.664 μg g^{-1}, [Nd] = 0.581 μg g^{-1}, $^{87}Sr/^{86}Sr = 0.702995$, $^{143}Nd/^{144}Nd = 0.513174$; Workman and Hart, 2005; Willhite *et al.*, 2019). Partial melting and fractional crystallisation, however, concentrates Sr and Nd in the melt, so endmember 2 provides an upper bound and assumes Sr and Nd concentrations similar to those found in the least contaminated lavas ([Sr] = 48.9 μg g^{-1}, [Nd] = 2.42 μg g^{-1}, $^{87}Sr/^{86}Sr = 0.702995$, $^{143}Nd/^{144}Nd = 0.513174$; Willhite *et al.*, 2019). Panel **(a)** shows the radiogenic isotopes of $^{87}Sr/^{86}Sr$ and $^{143}Nd/^{144}Nd$ with these endmembers, and **(b)** shows how these mixtures effect $\mu^{182}W$. Error bars are 2 s.d., and are smaller than the symbols for Sr and Nd isotopes. Mixing curves have hashes every 0.2 % additional crust.

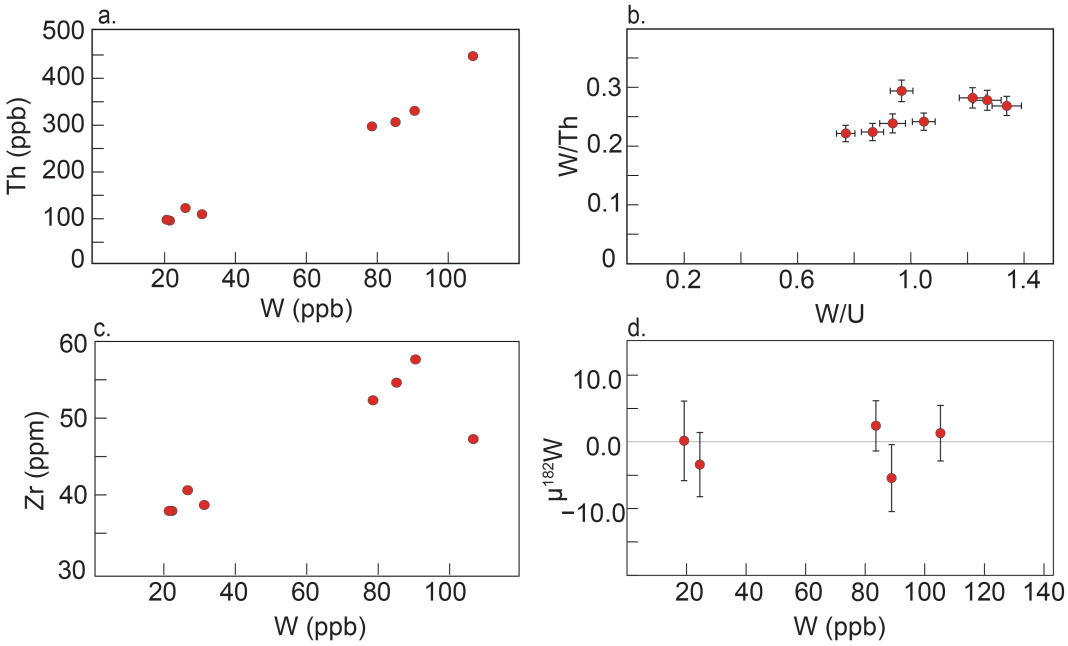

Figure S-4 Baffin Island $\mu^{182}W$ is invariant despite trace element variability. **(a)** Th (ng g^{-1}) *versus* W concentration (ng g^{-1}). Th and W have similar incompatibilities during igneous differentiation; however, W is more fluid-mobile than Th. The linear trend suggests that the W isotope systematics have not been affected by fluids. Uncertainties are smaller than the symbols. **(b)** W/Th *versus* W/U. Uranium, Th, and W are similarly incompatible during igneous differentiation, but U is more fluid mobile than W, which is more fluid mobile than Th. Again, fluid enrichment likely did not affect the W concentrations. Error bars reflect 2 s.d. uncertainties associated with W, Th, and U concentration measurements. **(c)** Zr (μg g^{-1}) *versus* W (ng g^{-1}) concentrations. Zr behaves incompatibly during igneous differentiation, so the range in W concentrations is probably the result of igneous differentiation. Uncertainties are smaller than the symbols. **(d)** W concentration (ng g^{-1}) *versus* $\mu^{182}W$. Error bars are 2 s.e. for the individual analysis.

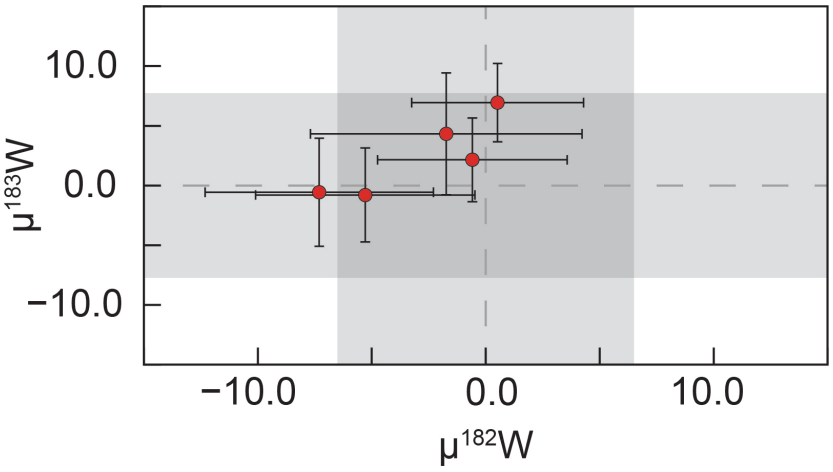

Figure S-5 $\mu^{183}W$ *versus* $\mu^{182}W$ for the five Baffin Island lava samples reported here. Error bars are 2 s.e. for each analysis. Grey regions represent the 2 s.d. of the primary standard, Alfa Aesar.

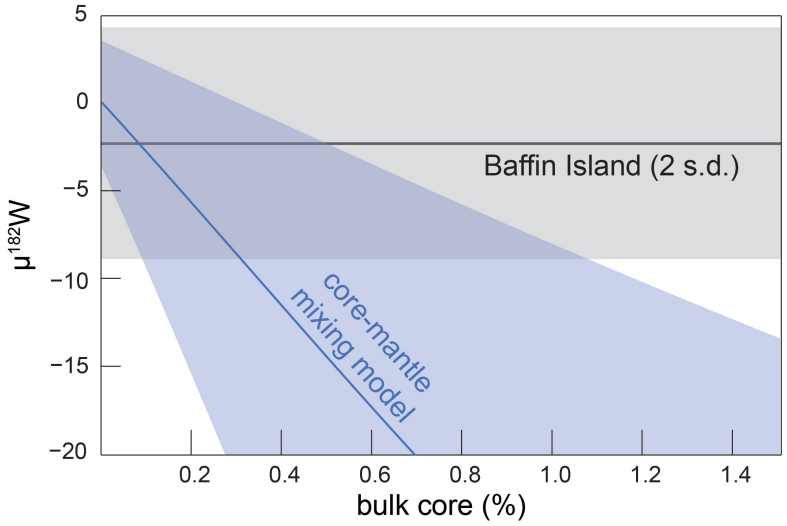

Figure S-6 Bulk mixing model (blue) between the core ($\mu^{182}W = -190 \pm 10$, 500 ± 120 ng g^{-1} W; Arevalo and McDonough, 2008; Kleine *et al.*, 2009) and depleted mantle ($\mu^{182}W = 0 \pm 3.5$, 29 ng g^{-1} W; McDonough and Sun, 1995; Rizo *et al.*, 2016; Mundl *et al.*, 2017). The shaded blue region represents the cumulative uncertainty associated with endmember concentrations and isotopic ratios, as well as mass balance. The grey line and shaded region represent the Baffin Island mean (−2.29, grey line) and 2 s.d. (±6.60, $n = 5$), respectively.

Supplementary Information References

Archer, G.J., Mundl, A., Walker, R.J., Worsham, E.A., Bermingham, K.R. (2017) High-precision analysis of $^{182}W/^{184}W$ and $^{183}W/^{184}W$ by negative thermal ionization mass spectrometry: Per-integration oxide corrections using measured $^{18}O/^{16}O$. *International Journal of Mass Spectrometry* 414, 80–86. https://doi.org/10.1016/j.ijms.2017.01.002

Arevalo Jr., R., McDonough, W.F. (2008) Tungsten geochemistry and implications for understanding the Earth's interior. *Earth and Planetary Science Letters* 272, 656–665. https://doi.org/10.1016/j.epsl.2008.05.031

Atreya, S.K., Mahaffy, P.R., Niemann, H.B., Wong, M.H., Owen, T.C. (2003) Composition and origin of the atmosphere of Jupiter—an update, and implications for the extrasolar giant planets. *Planetary and Space Science* 51, 105–112. https://doi.org/10.1016/S0032-0633(02)00144-7

Breton, T., Quitté, G. (2014) High-precision measurements of tungsten stable isotopes and application to earth sciences. *Journal of Analytical Atomic Spectrometry* 29, 2284–2293. https://doi.org/10.1039/C4JA00184B

Ferrick, A.L., Korenaga, J. (2023) Long-term core–mantle interaction explains W-He isotope heterogeneities. *Proceedings of the National Academy of Sciences* 120, e2215903120. https://doi.org/10.1073/pnas.2215903120

Hart, S.R., Kurz, M.D., Wang, Z. (2008) Scale length of mantle heterogeneities: Constraints from helium diffusion. *Earth and Planetary Science Letters* 269, 508–517. https://doi.org/10.1016/j.epsl.2008.03.010

Horton, F., Asimow, P.D., Farley, K.A., Curtice, J., Kurz, M.D., Blusztajn, J., Biasi, J., Boyes, X.M. (2023) Highest terrestrial $^{3}He/^{4}He$ credibly from the core. *Nature* 623, 90–94. https://doi.org/10.1038/s41586-023-06590-8

Kleine, T., Touboul, M., Bourdon, B., Nimmo, F., Mezger, K., Palme, H., Jacobsen, S.B., Yin, Q.-Z., Halliday, A.N. (2009) Hf–W chronology of the accretion and early evolution of asteroids and terrestrial planets. *Geochimica et Cosmochimica Acta* 73, 5150–5188. https://doi.org/10.1016/j.gca.2008.11.047

Kruijer, T.S., Kleine, T. (2018) No ^{182}W excess in the Ontong Java Plateau source. *Chemical Geology* 485, 24–31. https://doi.org/10.1016/j.chemgeo.2018.03.024

Kruijer, T.S., Sprung, P., Kleine, T., Leya, I., Burkhardt, C., Wieler, R. (2012) Hf–W chronometry of core formation in planetesimals inferred from weakly irradiated iron meteorites. *Geochimica et Cosmochimica Acta* 99, 287–304. https://doi.org/10.1016/j.gca.2012.09.015

Larsen, L.M., Pedersen, A.K. (2009) Petrology of the Paleocene Picrites and Flood Basalts on Disko and Nuussuaq, West Greenland. *Journal of Petrology* 50, 1667–1711. https://doi.org/10.1093/petrology/egp048

McDonough, W.F., Sun, S.-s. (1995) The composition of the Earth. *Chemical Geology* 120, 223–253. https://doi.org/10.1016/0009-2541(94)00140-4

Moreira, M.A., Kurz, M.D. (2013) Noble Gases as Tracers of Mantle Processes and Magmatic Degassing. In: Burnard, P. (Ed.) *The Noble Gases as Geochemical Tracers*. Advances in Isotope Geochemistry, Springer, Berlin, Heidelberg, 371–391. https://doi.org/10.1007/978-3-642-28836-4_12

Mundl, A., Touboul, M., Jackson, M.G., Day, J.M.D., Kurz, M.D., Lekic, V., Helz, R.T., Walker, R.J. (2017) Tungsten-182 heterogeneity in modern ocean island basalts. *Science* 356, 66–69. https://doi.org/10.1126/science.aal4179

Mundl-Petermeier, A., Walker, R.J., Jackson, M.G., Blichert-Toft, J., Kurz, M.D., Halldórsson, S.A. (2019) Temporal evolution of primordial tungsten-182 and $^{3}He/^{4}He$ signatures in the Iceland mantle plume. *Chemical Geology* 525, 245–259. https://doi.org/10.1016/j.chemgeo.2019.07.026

Mundl-Petermeier, A., Walker, R.J., Fischer, R.A., Lekic, V., Jackson, M.G., Kurz, M.D. (2020) Anomalous ^{182}W in high ^{3}He/^{4}He ocean island basalts: Fingerprints of Earth's core? *Geochimica et Cosmochimica Acta* 271, 194–211. https://doi.org/10.1016/j.gca.2019.12.020

Nagai, Y., Yokoyama, T. (2014) Chemical Separation of Mo and W from Terrestrial and Extraterrestrial Samples via Anion Exchange Chromatography. *Analytical Chemistry* 86, 4856–4863. https://doi.org/10.1021/ac404223t

Nakanishi, N., Puchtel, I.S., Walker, R.J., Nabelek, P.I. (2023) Dissipation of Tungsten-182 Anomalies in the Archean Upper Mantle: Evidence from the Black Hills, South Dakota, USA. *Chemical Geology* 617, 121255. https://doi.org/10.1016/j.chemgeo.2022.121255

Reimink, J.R., Mundl-Petermeier, A., Carlson, R.W., Shirey, S.B., Walker, R.J., Pearson, D.G. (2020) Tungsten Isotope Composition of Archean Crustal Reservoirs and Implications for Terrestrial μ^{182}W Evolution. *Geochemistry, Geophysics, Geosystems* 21, e2020GC009155. https://doi.org/10.1029/2020GC009155

Rizo, H., Walker, R.J., Carlson, R.W., Horan, M.F., Mukhopadhyay, S., Manthos, V., Francis, D., Jackson, M.G. (2016) Preservation of Earth-forming events in the tungsten isotopic composition of modern flood basalts. *Science* 352, 809–812. https://doi.org/10.1126/science.aad8563

Rizo, H., Andrault, D., Bennett, N.R., Humayun, M., Brandon, A., Vlastelic, I., Moine, B., Poirier, A., Bouhifd, M.A., Murphy, D.T. (2019) ^{182}W evidence for core-mantle interaction in the source of mantle plumes. *Geochemical Perspectives Letters* 11, 6–11. https://doi.org/10.7185/geochemlet.1917

Rudnick, R.L., Gao, S. (2003) 3.01 - Composition of the Continental Crust. In: Holland, H.D., Turekian, K.K. (Eds.) *Treatise on Geochemistry.* First Edition, Elsevier, Amsterdam, 1–64. https://doi.org/10.1016/B0-08-043751-6/03016-4

St-Onge, M.R., Van Gool, J.A.M., Garde, A.A., Scott, D.J. (2009) Correlation of Archaean and Palaeoproterozoic units between northeastern Canada and western Greenland: constraining the pre-collisional upper plate accretionary history of the Trans-Hudson orogen. In: Cawood, P.A., Kröner, A. (Eds.) *Earth Accretionary Systems in Space and Time*. Geological Society of London, London, 193–236. https://doi.org/10.1144/sp318.7

St-Onge, M.R., Scott, D.J., Rayner, N., Sanborn-Barrie, M., Skipton, D.R., Saumur, B.M., Wodicka, N., Weller, O.M. (2020) Archean and Paleoproterozoic cratonic rocks of Baffin Island. In: Dafoe, L.T., Bingham-Koslowski, N. (Eds.) *Geological Survey of Canada, Bulletin 608*. Geological Survey of Canada, Montreal, 25–53. https://doi.org/10.4095/321824

Touboul, M., Walker, R.J. (2012) High precision tungsten isotope measurement by thermal ionization mass spectrometry. *International Journal of Mass Spectrometry* 309, 109–117. https://doi.org/10.1016/j.ijms.2011.08.033

Völkening, J., Köppe, M., Heumann, K.G. (1991) Tungsten isotope ratio determinations by negative thermal ionization mass spectrometry. *International Journal of Mass Spectrometry and Ion Processes* 107, 361–368. https://doi.org/10.1016/0168-1176(91)80070-4

Willhite, L.N., Jackson, M.G., Blichert-Toft, J., Bindeman, I., Kurz, M.D., Halldórsson, S.A., Harðardóttir, S., Gazel, E., Price, A.A., Byerly, B.L. (2019) Hot and Heterogenous High-^{3}He/^{4}He Components: New Constraints From Proto-Iceland Plume Lavas From Baffin Island. *Geochemistry, Geophysics, Geosystems* 20, 5939–5967. https://doi.org/10.1029/2019GC008654

Workman, R.K., Hart, S.R. (2005) Major and trace element composition of the depleted MORB mantle (DMM). *Earth and Planetary Science Letters* 231, 53–72. https://doi.org/10.1016/j.epsl.2004.12.005

Yoshino, T., Makino, Y., Suzuki, T., Hirata, T. (2020) Grain boundary diffusion of W in lower mantle phase with implications for isotopic heterogeneity in oceanic island basalts by core-mantle interactions. *Earth and Planetary Science Letters* 530, 115887. https://doi.org/10.1016/j.epsl.2019.115887